Journal of Alloys and Compounds 509 (2011) 2808–2814

Contents lists available at ScienceDirect

Journal of Alloys and Compounds

journal homepage: www.elsevier.com/locate/jallcom

An investigation on hydrogen storage kinetics of nanocrystalline and amorphous $Mg_2Ni_{1-x}Co_x$ ($x = 0$–0.4) alloy prepared by melt spinning

Yang-huan Zhang[a,b,*], Bao-wei Li[a], Hui-pin Ren[a], Xiao-xia Ding[a,b], Xiao-gang Liu[a,b], Le-le Chen[a,b]

[a] Elected State Key Laboratory, Inner Mongolia University of Science and Technology, Baotou 014010, China
[b] Department of Functional Material Research, Central Iron and Steel Research Institute, Beijing 100081, China

ARTICLE INFO

Article history:
Received 14 September 2010
Received in revised form
12 November 2010
Accepted 17 November 2010
Available online 24 November 2010

Keywords:
Mg_2Ni-type alloy
Melt spinning
Substituting Ni with Co
Hydrogen storage kinetics

ABSTRACT

In order to improve the hydrogen storage kinetics of the Mg_2Ni-type alloys, Ni in the alloy was partially substituted by element Co, and melt-spinning technology was used for the preparation of the $Mg_2Ni_{1-x}Co_x$ ($x = 0, 0.1, 0.2, 0.3, 0.4$) hydrogen storage alloys. The structures of the as-cast and spun alloys are characterized by XRD, SEM and TEM. The hydrogen absorption and desorption kinetics of the alloys were measured by an automatically controlled Sieverts apparatus. The electrochemical hydrogen storage kinetics of the as-spun alloys is tested by an automatic galvanostatic system. The hydrogen diffusion coefficients in the alloys are calculated by virtue of potential-step method. The electrochemical impedance spectrums (EIS) and the Tafel polarization curves are plotted by an electrochemical workstation. The results show that the substitution of Co for Ni notably enhances the glass forming ability of the Mg_2Ni-type alloy. Furthermore, the substitution of Co for Ni, instead of changing major phase Mg_2Ni, leads to forming secondary phases $MgCo_2$ and Mg. Both the melt spinning treatment and Co substitution significantly improve the hydrogen absorption and desorption kinetics. The high rate discharge ability, the hydrogen diffusion coefficient and the limiting current density of the alloys significantly increase with raising both the spinning rate and the amount of Co substitution.

1. Introduction

Mg and Mg-based metallic hydrides are considered to be more promising materials for hydrogen storage because of their major advantages such as low specific weight, low cost and high hydrogen capacity, e.g. 7.6 wt.% for MgH_2, 3.6 wt.% for Mg_2NiH_4 [1,2]. However, their practical application to hydrogen suppliers has been limited mainly due to their sluggish hydriding/dehydriding kinetics as well as high thermodynamic stability of their corresponding hydride. To achieve the application goal, a variety of attempts, involving mechanical alloying (MA) [3], melt spinning [4,5], surface modification [6], adding catalysts [7,8], hydriding combustion synthesis [9], alloying with other elements [10], GPa hydrogen pressure method [11] etc., have been developed and employed to ameliorate the kinetics of Mg-based metallic hydrides. It was documented that the researches in this area have achieved great progress in hydrogen absorption/desorption kinetics of Mg-based alloys. However, thermodynamic stability and decomposition temperature of Mg based hydrides are still too high for their practical utilization as hydrogen accumulators. Therefore, the scientists in this field still continue their attempts towards decreasing thermal stability of the Mg-based hydride.

Especially, high energy ball-milling, a very powerful method for the preparation of nanocrystalline and amorphous Mg and Mg-based alloys, is quite suitable to solubilize particular elements into MgH_2 or Mg_2NiH_4 above the thermodynamic equilibrium limit, which may facilitate to destabilize MgH_2 or Mg_2NiH_4 [12]. However, the milled Mg and Mg-based alloys show extremely poor hydrogen absorbing and desorbing cycle stability due to the fact that the metastable structures produced by ball milling tended to vanish during multiple hydrogen absorbing and desorbing cycles [13], which is an insurmountable bottleneck for their practical applications.

Alternatively, melt-spun technique can overcome the above mentioned shortcoming and effective restraining the rapid degradation of hydrogen absorbing and desorbing cycle properties of Mg and Mg-based [14]. Furthermore, the alloys, possessing the nanocrystalline and amorphous structure produced by melt-spinning method, exhibit excellent initial electrochemical hydrogen storage characteristics similar to those of the alloys fabricated by the MA process. Tanaka et al. [15] prepared the $Mg_{85}Ni_{10}La_5$ hydrogen storage alloy with a nanostructure by melt spinning to obtain reversible absorption and desorption amount of about 5 wt.% hydrogen at temperatures as low as 200 °C in moderate time periods. Spassov et al. [16] have prepared Mg_2 (Ni, Y) hydrogen storage alloy with the composition of $Mg_{63}Ni_{30}Y_7$

* Corresponding author at: Department of Functional Material Research, Central Iron and Steel Research Institute, 76 Xueyuan Nan Road, Haidian District, 100081 Beijing, China. Tel.: +86 010 62187570; fax: +86 010 62183115.
E-mail address: zyh59@yahoo.com.cn (Y.-h. Zhang).

0925-8388/$ – see front matter © 2010 Elsevier B.V. All rights reserved.
doi:10.1016/j.jallcom.2010.11.113

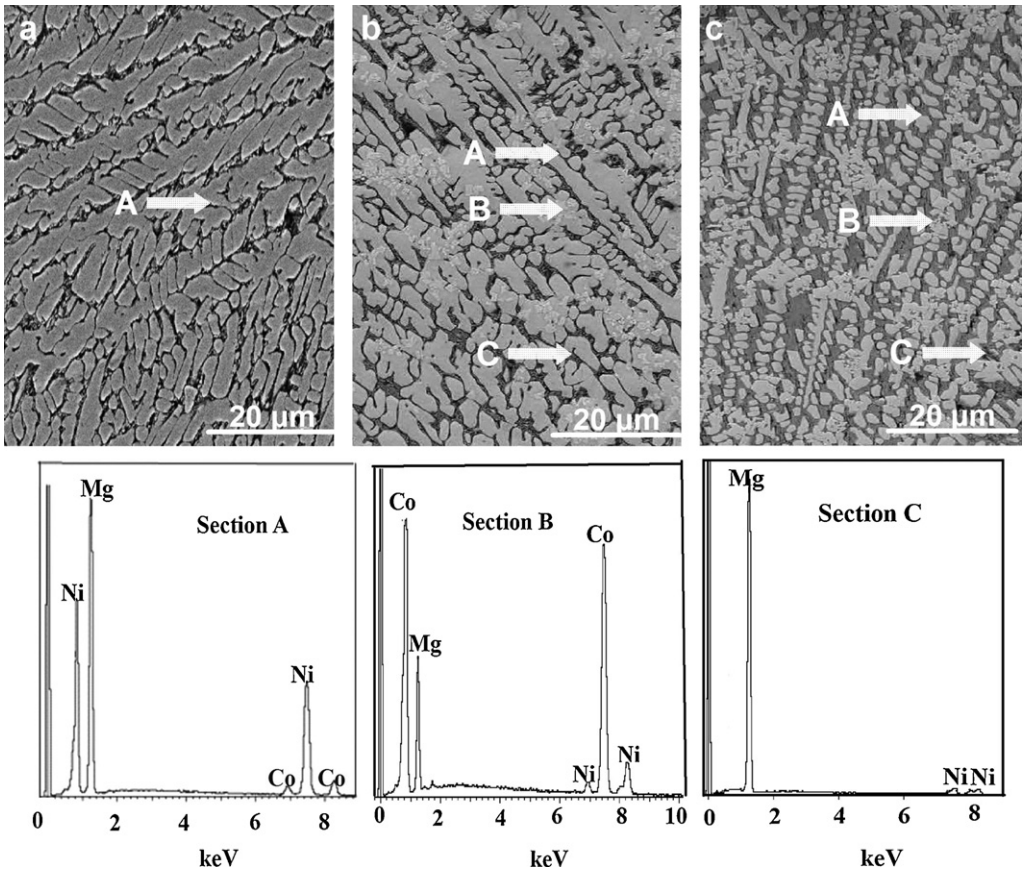

Fig. 1. SEM images of the Co_0, $Co_{0.1}$ and $Co_{0.3}$ alloys together with typical EDS spectra of sections A and B in (b): (a) Co_0 alloy, (b) $Co_{0.1}$ alloy, (c) $Co_{0.3}$ alloy.

by rapid solidification process, exhibiting a maximum hydrogen absorption capacity of about 3.0 wt%. In addition, the melt-spun Mg_2 (Ni, Y) alloys have demonstrated an enhanced hydrogenation kinetics compared to those of the conventionally prepared polycrystalline Mg_2Ni alloys, to be comparable to that of the nanocrystalline ball-milled Mg_2Ni.

In the present work, the Mg-Ni-based $Mg_2Ni_{1-x}Co_x$ ($x = 0$–0.4) nanocrystalline and amorphous alloys have been synthesized by melt-spinning technology. Moreover, the effects of both spinning rate and Co content on the structures and hydrogen storage kinetics of the alloys have been investigated in detail.

2. Experimental

The experimental alloys were prepared by using a vacuum induction furnace in a helium atmosphere at a pressure of 0.04 MPa. A part of the as-cast alloys was remelted and spun by melt-spinning with a rotating copper roller cooled by water. The as-spun alloy ribbons, having a continuous length, a thickness of about 30 μm and a width of about 25 mm, are obtained. The spinning rate was approximately expressed by the linear velocity of the copper roller. The spinning rates used in the experiment were15, 20, 25 and 30 m/s, respectively. The nominal compositions of the experimental alloys were $Mg_2Ni_{1-x}Co_x$ ($x = 0$, 0.1, 0.2, 0.3, 0.4). For convenience, the alloys were denoted with Co content as Co_0, $Co_{0.1}$, $Co_{0.2}$, $Co_{0.3}$ and $Co_{0.4}$, respectively.

A Philips SEM (QUANTA 400) linked with an energy dispersive spectrometer (EDS) was used for morphological characterization and chemical analysis of the as-cast alloys.

The phase structures of the as-cast and spun alloys were determined by X-ray diffraction (XRD) (D/max/2400). The diffraction, with the experimental parameters of 160 mA, 40 kV and 10°/min respectively, was performed with $CuK_{\alpha 1}$ radiation filtered by graphite. The effective grain sizes were calculated from Scherrer's formula [17].

The thin film samples of the as-spun alloys were prepared by ion etching method in order to observe the morphology with high resolution transmission electron microscope (HRTEM) (JEM-2100F, operated at 200 kV), and also to determine the crystalline state of the samples with electron diffraction (ED). The average grain sizes of the as-spun alloys were measured by a linear intercept method on the HRTEM micrographs.

The hydrogen absorption and desorption kinetics of the alloys were measured by an automatically controlled Sieverts apparatus. Prior to measuring the hydriding and dehydriding kinetics of the alloys, several hydrogen absorbing and desorbing cycles were performed in order to activate the materials. The hydrogen absorption was conducted at 1.5 MPa and 200 °C, and the hydrogen desorption at a pressure of 1×10^{-4} MPa and 200 °C.

The alloy ribbons were pulverized into fine powder of about 20 μm by mechanical milling and then mixed with carbonyl nickel powder in a weight ratio of 1:4. The mixture was cold pressed under a pressure of 35 MPa into round electrode pellets of 10 mm in diameter and total mass of about 1 g. The electrochemical hydrogen storage kinetics of the alloy electrodes were tested by a tri-electrode open cell, consisting of a metal hydride electrode, a sintered $NiOOH/Ni(OH)_2$ counter electrode and a Hg/HgO reference electrode. The electrolyte is a solution of 6 M KOH. The voltage between the negative electrode and the reference electrode was defined as the discharge voltage. In every cycle, the alloy electrode was first charged at a constant current density, and following the resting for 15 min, it was discharged at the same current density to −0.500 V cut-off voltage. The environment temperature of the measurement was kept at 30 °C.

The electrochemical impedance spectra (EIS) and the Tafel polarization curves of the alloys were measured using an electrochemical workstation (PARSTAT 2273). The fresh electrodes were fully charged and then rested for 2 h up to the stabilization of the open circuit potential. The EIS spectra of the alloy electrodes were measured in the frequency range from 10 kHz to 5 mHz at 50% depth of discharge (DOD). The Tafel polarization curves were measured in the potential range of −1.2 to +1.0 V (vs. Hg/HgO) with a scan rate of 5 mV/s. For the potentiostatic discharge, the test electrodes in the fully charged state were discharged at 500 mV potential steps for 4500 s on electrochemical workstation (PARSTAT 2273), using the CorrWare electrochemistry corrosion software.

3. Results

3.1. Structural characteristics

Depicted in Fig. 1 are the SEM images of the as-cast Co_0, $Co_{0.1}$ and $Co_{0.3}$ alloys. It is very evident that the substitution of Co for Ni causes the visible refinement of the grains of the as-cast alloy. The morphologies of the as-cast alloys exhibit primary crystals of Mg_2Ni

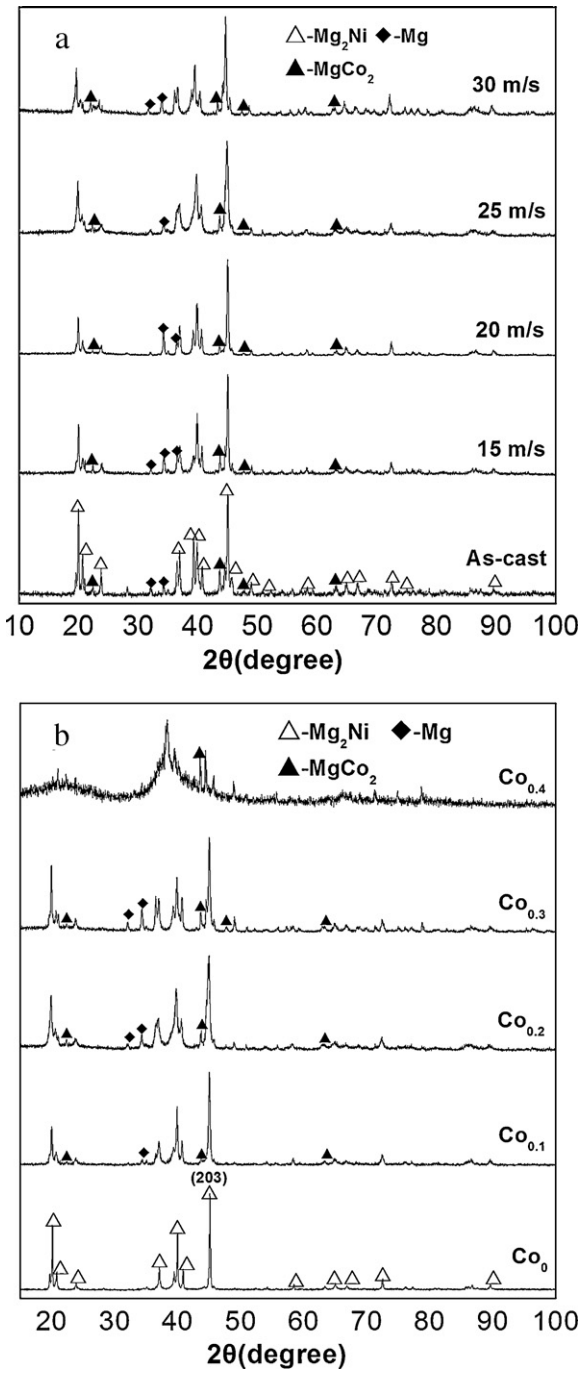

Fig. 2. XRD profiles of the as-cast and spun alloys: (a) $Co_{0.2}$ alloy, (b) As-spun (25 m/s).

(light) and a eutectic (dark) consisting of Mg, Mg_2Ni and $MgCo_2$. The result obtained by energy dispersive spectrometry (EDS) indicates that, instead of altering the major phase Mg_2Ni (denoted by A) in the alloys, the substitution of Co for Ni leads to forming secondary phases $MgCo_2$ (denoted by B) and Mg (denoted by C).

The XRD profiles of the as-cast and spun alloys are illustrated in Fig. 2. The figure displays that the as-cast and spun alloys have a multiphase structure, comprising of a major phase Mg_2Ni and secondary phases $MgCo_2$ and Mg. The melt spinning treatment has an unapparent influence on the structure of the $Co_{0.2}$ alloy, while it causes a great change of the structure of the $Co_{0.4}$ alloy. As the spinning rate reaches to 25 m/s, the $Co_{0.4}$ alloy exhibits an obvious amorphous structure, confirming that the substitution of Co for Ni facilitates the glass formation in the Mg_2Ni-type alloy. Listed in Table 1 are the lattice parameters, cell volumes and full width at half maximum (FWHM) values of the main diffraction peaks of the as-spun (25 m/s) alloys which were calculated by using Jade 6.0 software. It is derived in Table 1 that the increase in the amount of Co substitution causes not only an visible increase in the FWHM values of the main diffraction peaks of the as-spun alloys but also an evident enlargement in the lattice parameters and cell volume of the alloys, to be attributed to the larger atomic radius of Co than Ni. Based on the FWHM values of the broad diffraction peak (2 0 3) in Fig. 2(b), the grain sizes $\langle D_{hkl}\rangle$ (nm) of the as-spun (25 m/s) alloys are calculated using Scherrer's equation, also listed in Table 1. It reveals that the substitution of Co for Ni causes an obvious reduction of the grain sizes of the alloys.

Table 1
Lattice parameters, cell volumes, FWHM values and grain sizes of the as-spun (25 m/s) alloys.

Alloys	FWHM values	Grain sizes	Lattice parameters and cell volumes		
	2θ (45.14°)	D_{203} (nm)	a (nm)	c (nm)	V (nm^3)
Co_0	0.179	48	0.5211	1.3265	0.3121
$Co_{0.1}$	0.310	27	0.5219	1.3318	0.3149
$Co_{0.2}$	0.425	20	0.5225	1.3323	0.3150
$Co_{0.3}$	0.461	18	0.5226	1.3401	0.3169
$Co_{0.4}$	–	–	–	–	–

The TEM micrographs and ED patterns of the as-spun (25 m/s) alloys are demonstrated in Fig. 3. It is clearly viewable that the as-spun $Co_{0.1}$ alloy displays a nearly complete nanocrystalline structure, and its electron diffraction (ED) pattern appears sharp multi-haloes, corresponding to a crystalline structure, while the $Co_{0.4}$ alloy exhibits a clear feature of the nanocrystalline embedded in the amorphous matrix, and its electron diffraction pattern consisted of broad and dull halo, confirming the presence of an amorphous structure. It is quite evident that the amorphization degree of the as-spun alloys visibly increases with the increase in the amount of Co substitution, which conforms to the XRD observations depicted in Fig. 2.

3.2. Hydrogen absorption and desorption kinetics

The hydrogen absorption was carried out under 1.5 MPa hydrogen pressure (in fact, this pressure is initial pressure of hydriding process), and hydrogen desorption was performed in an initial pressure of 1×10^{-4} MPa at 200 °C.

The hydrogen absorption kinetics of the alloy is signified by hydrogen absorption saturation ratio (R_t^a), being defined as $R_t^a = C_t^a/C_{100}^a \times 100\%$, where C_{100}^a and C_t^a are hydrogen absorption capacities in the time of 100 min and t min, respectively. Apparently, for a fixed time t, a larger saturation ratio R_t^a means better hydrogen absorption kinetics. The experimental result indicates that, for all the experimental alloys, the C_{100}^a values are more than 98% of their saturated hydrogen absorption capacities. Therefore, it is reasonable to take the C_{100}^a value as the saturated hydrogen absorption capacity of the alloy. The evolution of the hydrogen absorption saturation ratio (R_t^a) ($t = 5$) of the alloys with the spinning rate is presented in Fig. 4. The figure reveals that the R_5^a values of the alloys notably increase with rising spinning rate. With an increase in the spinning rate from 0 (As-cast is defined as spinning rate of 0 m/s) to 30 m/s, the R_5^a value increases from 80.4 to 94.3% for the $Co_{0.2}$ alloy. As the amount of Co substitution rises from 0 to 0.4, the R_5^a value of the as-spun (25 m/s) increases from 89.0 to 91.8%. It is noteworthy that the difference of the R_5^a values of the alloys clearly reduces with rising spinning rate. When the spinning rate reaches to 30 m/s, all the alloys show a nearly same R_5^a value, suggesting that the hydro-

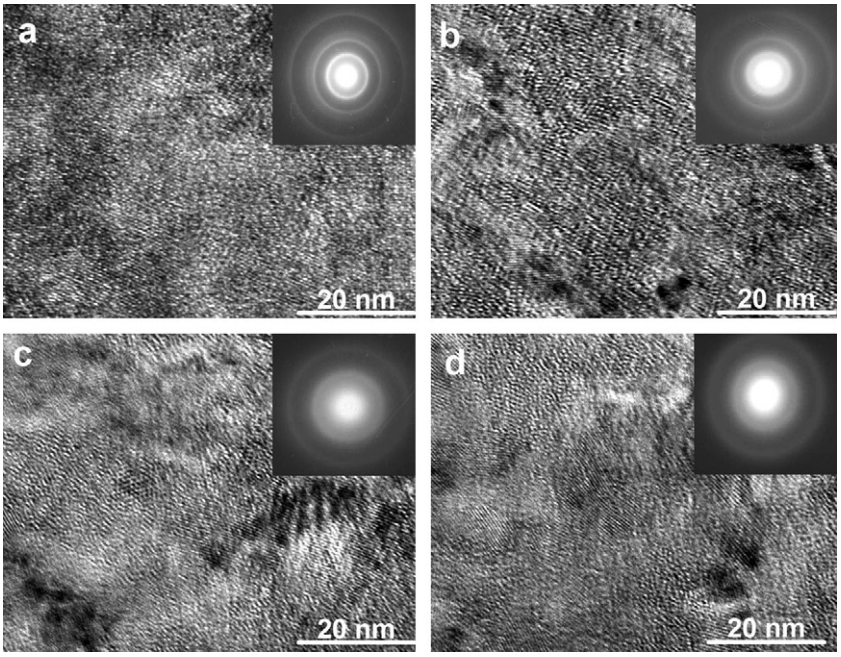

Fig. 3. HRTEM micrographs and ED patterns of the as-spun (25 m/s) alloy: (a) $Co_{0.1}$ alloy, (b) $Co_{0.2}$ alloy, (c) $Co_{0.3}$ alloy, (d) $Co_{0.4}$ alloy.

gen absorption kinetics of the as-spun alloy chiefly depends on its structure.

Similarly, the hydrogen desorption kinetics of the alloy is indicated by hydrogen desorption ratio (R_t^d), being defined as $R_t^d = C_t^d/C_{100}^a \times 100\%$, where C_{100}^a is the hydrogen absorption capacity in 100 min and C_t^d is the hydrogen desorption capacity in the time of t min, respectively. The evolution of the hydrogen desorption ratio (R_{20}^d) ($t = 20$) of the alloys with the spinning rate is illustrated in Fig. 5. It can be seen in Fig. 5 that the melt spinning treatment remarkably enhances the R_{20}^d values of the alloys, suggesting that melt spinning facilitates hydrogen desorption of Mg_2Ni-type alloy. With the increase in the spinning rate from 0 to 30 m/s, the R_{20}^d value of the $Co_{0.2}$ alloy increases from 24.52 to 51.67%. It must be mentioned that, for a fixed spinning rate, the R_{20}^d value of the alloy markedly increases with the increase in the amount of Co substitution.

3.3. Electrochemical hydrogen storage kinetics

Electrochemical galvanostatic charge/discharge is a more effective and less time-consuming method for determining the hydrogen storage kinetics than a gaseous technique. It is quite important to restrict the rapid attenuation in the discharge capacity even at a high charge/discharge current density for the practical application of hydride electrode in Ni–MH battery. Usually, the electrochemical kinetics of the alloy is characterized by its high rate discharge ability (HRD), being calculated according to following formula: $HRD = C_{i\,max}/C_{20,max} \times 100\%$, where $C_{i,max}$ and $C_{20,max}$ are the maximum discharge capacities of the alloy electrode charged-discharged at the current densities of i and 20 mA/g respectively.

The relationship between the HRD values of the as-cast and spun alloys with the discharge current density is exhibited in Fig. 6. The figure shows that the HRD values of all the alloys increase with rising both spinning rate and Co content. As the spinning rate rises from 0 to 30 m/s, the HRD value ($i = 100$ mA/g) of the $Co_{0.2}$ alloy increases from 56.7 to 71.7%. And the HRD value ($i = 100$ mA/g) of the as-spun (25 m/s) alloy raises from 65.3 to 75.3% with a increase in the amount of Co substitution from 0 to 0.4.

In order to reveal the mechanism of both melt spinning and Co substitution improving hydrogen absorption kinetics of the alloy, it is evidently necessary to investigate the influences of the melt spinning and Co substitution on the H diffusion ability in the alloy. The H

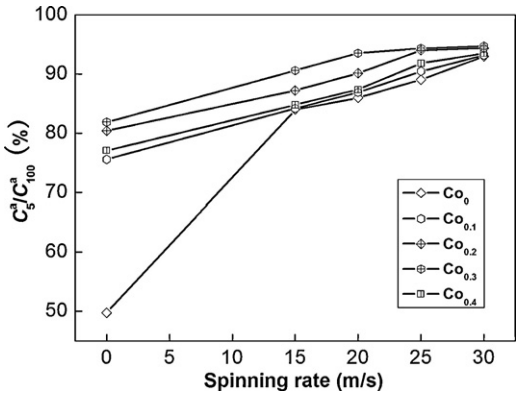

Fig. 4. Evolution of the hydrogen absorption saturation ratio (R_5^a) of the alloys with the spinning rate.

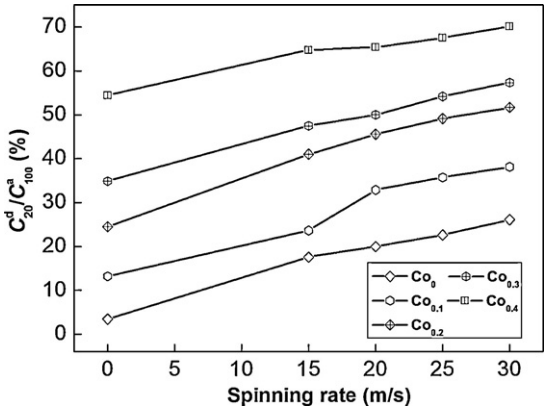

Fig. 5. Evolution of the hydrogen desorption ratio (R_{20}^d) of the alloys with the spinning rate.

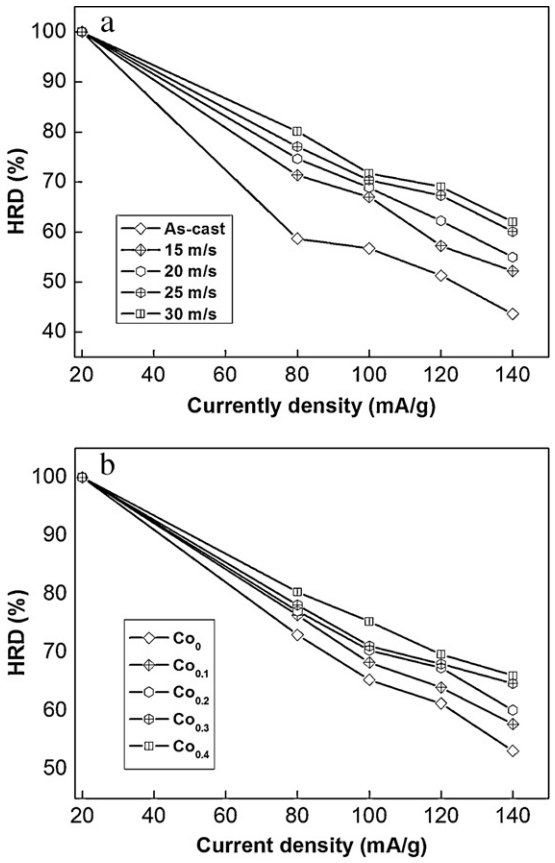

Fig. 6. Evolution of the high rate discharge ability (HRD) of the alloys with the discharge current density: (a) $Co_{0.2}$ alloy, (b) As-spun (25 m/s).

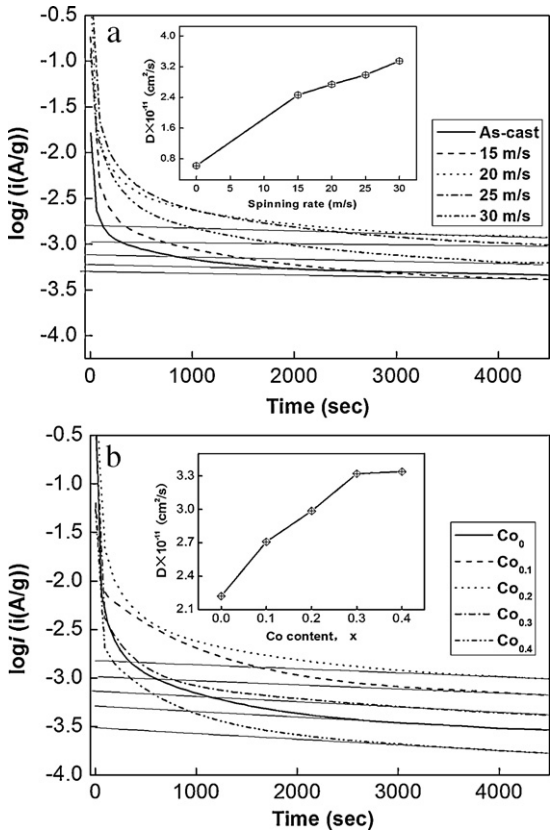

Fig. 7. Semilogarithmic curves of anodic current vs. time responses of the alloys: (a) $Co_{0.2}$ alloy; (b) As-spun (25 m/s).

diffusion coefficients in the as-cast and spun alloys were measured using the potential step technique. A potential step of +500 mV versus the stabilized open circuit potential of the fully charged electrode was applied and the decrease in discharge current was monitored as a function of time. Fig. 7 presents the semilogarithmic curves of anodic current versus working duration of the as-cast and spun alloys. The diffusion coefficient D of hydrogen atoms in the bulk of the alloy can be calculated through the slope of the linear region of the corresponding plots according to following formulae [18].

$$\log i = \log\left(\pm\frac{6FD}{da^2}(C_0 - C_s)\right) - \frac{\pi^2}{2.303}\frac{D}{a^2}t \quad (1)$$

$$D = -\frac{2.303a^2}{\pi^2}\frac{\mathrm{d}\log i}{\mathrm{d}t} \quad (2)$$

where i is the diffusion current density (A/g), D is the hydrogen diffusion coefficient (cm^2/s), C_0 is the initial hydrogen concentration in the bulk of the alloy (mol/cm^3), C_s is the hydrogen concentration on the surface of the alloy particles (mol/cm^3), a is the alloy particle radius (cm), d is the density of the hydrogen storage alloy (g/cm^3), t is the discharge time (s), respectively. In Eq. (2), $\mathrm{d}\log i/\mathrm{d}t$ is the slope of the linear region of the semilogarithmic curves of anodic current versus working duration, which can easily be obtained by using origin 75 software. a is the alloy particle radius, supposing $a = 15\ \mu m$. Thus, hydrogen diffusion coefficient D can easily be obtained. The D values calculated by Eq. (2) are also shown in Fig. 7. It is quite evident that an increase in the spinning rate turns out a notable rise in the D value. As the spinning rate rises from 0 to 30 m/s, the D value increases from 6.23×10^{-12} to 3.35×10^{-11} cm^2/s for the $Co_{0.2}$ alloy. And the D value of the as-spun (25 m/s) alloys mounts up from 2.22×10^{-11} to 3.34×10^{-11} cm^2/s with an increase in the amount of Co substitution from 0 to 0.4.

To determine the kinetics of hydrogen absorption/desorption, Tafel polarization measurements are carried out on the experimental alloy electrodes. Fig. 8 illustrates the Tafel polarization curves of the as-cast and spun alloy electrodes at the 50% DOD. It shows that, in all cases, the anodic current densities increase to a limiting value, then decrease. The existence of a limiting current density, I_L, indicates the formation of an oxidation layer on the surface of the alloy electrode, which resists further penetration of hydrogen atoms [19]. The decrease of the anodic charge current density on cycling implies that charging was becoming more difficult. Hence, the limiting current density, I_L, may be regarded as a critical passivation current density. Fig. 8(a) exhibits that I_L values of the alloys notably increase with rising spinning rate. With an increase in the spinning rate from 0 to 30 m/s, the I_L value increases from 57.5 to 772.3 mA/g for the $Co_{0.2}$ alloy. Fig. 8(b) reveals that the I_L value of the as-spun (25 m/s) alloys enhances from 247.9 to 712.4 mA/g as the amount of Co substitution rises from 0 to 0.4. Furthermore, an interesting phenomenon in Fig. 8 displays that the corresponding peak potential of the limiting current apparently shifts to positive direction with the increase of both spinning rate and Co content, indicating an enhanced antioxidation or anticorrosion ability by both the melt spinning and Co substitution.

Shown in Fig. 9 are the electrochemical impedance spectra (EIS) of the as-cast and spun alloy electrodes at 50% DOD. It is viewable that each EIS spectrum contains two semicircles followed by a straight line. According to Kuriyama et al.'s opinion, [20] the smaller semicircle in the high frequency region is attributed to the contact resistance between the alloy powder and the conductive material, while the larger semicircle in the low frequency region is attributed to the charge-transfer resistance on the alloy surface. The linear

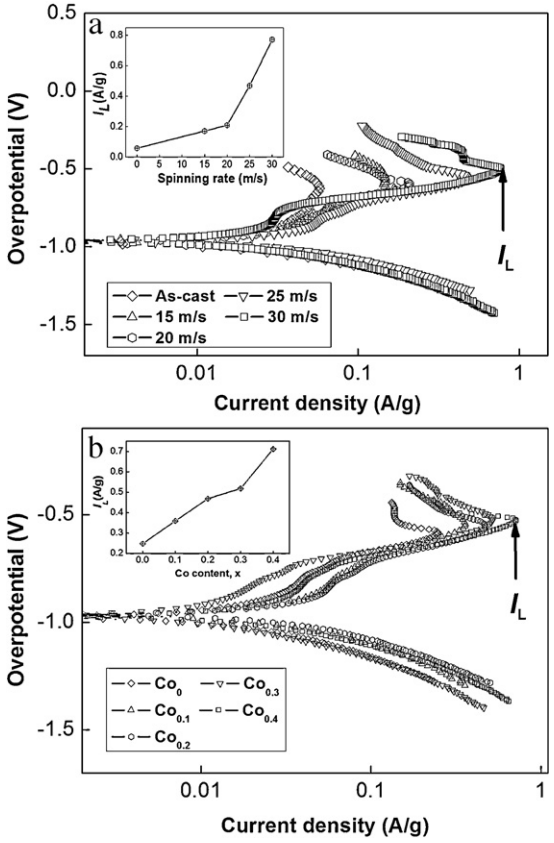

Fig. 8. Tafel polarization curves of the as-cast and spun alloy electrodes at the 50% DOD: (a) Co0.2 alloy; (b) As-spun (25 m/s).

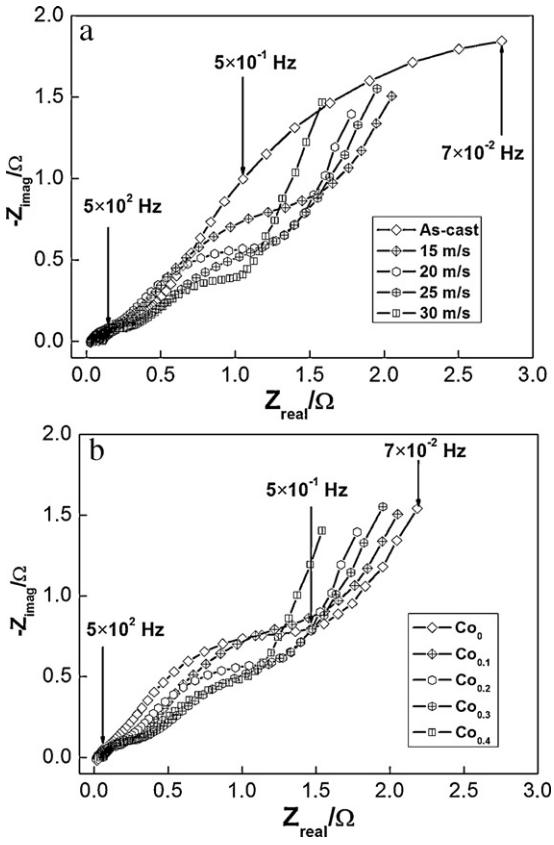

Fig. 9. Electrochemical impedance spectra (EIS) of the alloy electrodes at the 50% depth of discharge (DOD): (a) Co0.2 alloy, (b) As-spun (25 m/s).

response at low frequencies is indicative of hydrogen diffusion in the bulk alloy. Hence, the electrode kinetics of the as-cast and spun alloys are dominated a mixed rate-determining process. It is seen in Fig. 9 that the radius of the large semicircle in the low frequency for the as-cast and spun alloys visibly decreases with increasing both spinning rate and Co content, implying that the refined grain by both the melt spinning and Co substitution facilitates charge-transfer of the alloy electrode.

4. Discussion

Based on a systematic investigation on the structures of the $Mg_2Ni_{1-x}Co_x$ (x = 0–0.4) alloys, some explanations may be offered as the reasons of the melt spinning and the substitution of Co for Ni leading to the notable changes of the structure and hydrogen storage kinetics of the Mg_2Ni-type alloy.

The results as shown in Figs. 2 and 3 reveal that the substitution of Co for Ni facilitates the glass formation in the Mg_2Ni-type alloy, for which two possibilities are mainly responsible. On the one hand, the addition of third element to Mg–Ni or Mg–Cu alloys can significantly facilitate the glass-formation [21,22]. On the other hand, the glass forming ability of the alloy is closely related to the difference of the atom radius of the alloy. The bigger the difference of the atom radius prefigures the higher the glass forming ability of the alloy [23]. It must be mentioned that the structure of the alloy with a fixed composition basically depends on its preparation technology. A lot of literatures have reported that melt spinning can leads to a marked refinement of the grains in the alloy. The similar results have been obtained by our group [24]. The grain sizes of the alloy are closely related to the spinning rate. The higher spinning rate will create the smaller grain size.

Generally, the diffusion ability of hydrogen atoms in the alloy is a crucial factor for the hydrogen absorption kinetics. The melt spinning treatment markedly enhances the hydrogen absorption kinetics (Fig. 4). The improved hydrogen absorption kinetics is mainly ascribed to the enhanced hydrogen diffusivity in the amorphous and nanocrystalline microstructures as the amorphous phase around the nanocrystalline leads to an easier access of hydrogen to the nanograins, avoiding the long-range diffusion of hydrogen through an already formed hydride, which is often the slowest stage of absorption. Upon refining the microstructure, a lot of new crystallites and grain boundaries evolve, which may act as fast diffusion paths for hydrogen absorption [25]. It is quite evident that the positive function of Co substitution on the R_5^a value of the alloy clearly decreases with increasing spinning rate. As the spinning rate reaches to 30 m/s, the all the alloys have nearly same R_5^a values. It reveals that the hydrogen absorption kinetics of the as-spun alloy basically depends on its structure.

It is well known that the hydrogen desorption kinetics of the alloy primarily relies on the hydrogen diffusion ability as well as the thermal stability of its hydride. The poor hydriding/dehydriding kinetics of the Mg and Mg-based alloys is principally ascribed to the high thermodynamic stability of their corresponding hydride. The improved hydrogen desorption kinetics is mostly associated with the change of the structure of the alloy induced by the melt spinning. It is well known that, when crystalline materials are spun, they become at least partially disordered. And at same time, some crystal defects such as dislocations, stacking faults and grain boundaries are introduced. As a result, a large amount of internal energy would be stored and lead to non-stabilization of the lattice, yielding the nanocrystalline or even an amorphous phase. Niu et al. [19] clarified that the introduction of defects, disordering and internal strain gives rise to an increasing hydriding/dehydriding rates and capacity. It was reported [25] that the hydrogen absorbing and desorbing rates of Mg-based alloys were strongly enhanced

by refinement of the grains. As noted, the internal strain increases with rising spinning rate. The higher the spinning rate, the more defects are introduced into the Mg_2Ni alloy. Furthermore, the grain size of the alloy markedly decreases with increasing spinning rate. Hence, it is understandable that the hydrogen desorption ratio (R^d_{20}) of the alloy markedly increases with rising spinning rate. It is noteworthy that, for a fixed spinning rate, the R^d_{20} value of the alloy marked increase with rising Co content, suggesting that increasing Co content facilitates hydrogen desorption. The increased hydrogen desorption kinetics by Co substitution is ascribed to two reasons. Firstly, the substitution of Co for Ni notably intensifies the glass forming ability of Mg_2Ni-type alloy because amorphous Mg_2Ni shows an excellent hydrogen desorption capability. Secondly, such substitution decreases the stability of the hydride and makes the desorption reaction easier [26]. It is must be pointed out that the total hydrogen storage capacities of the experimental alloys under our test conditions are not as large as would be found fromMg_2NiH_4. It was confirmed by our previous work [27] that the products of the hydriding reaction of the as-cast and spun alloys are $Mg_2NiH_4 + MgH_2 + MgCo_2$ and that the products of the dehydriding reaction of the alloys are $Mg_2Ni + MgH_2 + MgCo_2$. The formation of MgH_2 phase is probably relevant to the substitution of Co for Ni. The low hydrogen absorption capacity of the as-cast and spun is ascribed to the formation of the Mg_2Co phase because it is not a hydride forming phase. And low hydrogen desorption capacity of the alloys is attribute to the formation of the MgH_2 phase owing to the fact that the thermal stability of the MgH_2 phase is higher than that of the Mg_2NiH_4 phase and it keeps unreaction under our test conditions.

High rate dischargeability (HRD) is a kinetic performance of hydrogen absorbing/desorbing of the alloy electrode, which principally depends on the charge transfer at the alloy-electrolyte interface the hydrogen diffusion process from the interior of the bulk to the surface of alloy particle [28]. The radiuses of the larger semicircle on the EIS spectra in the low frequency region exhibit a same change with the HRD values of the alloys, indicating that the HRD values of the alloy electrodes is directly associated with the charge-transfer resistance of the alloy. Figs. 7 and 8 indicate that the diffusion coefficient (D) of hydrogen and the limiting current density (I_L) visibly increase with rising spinning rate and Co content. Ratnakumar et al. [29] and Liu et al. [30] presumed that the limiting current can be related to and is mainly controlled by the solid state diffusion of hydrogen in metal-hydride electrode. Furthermore, it was known that the limiting current density, I_L, may be regarded as a critical passivation current density. The results shown in Figs. 2 and 3 indicate that the glass forming ability of the Mg_2Ni-type alloy can significantly be enhanced by both increasing spinning rate and Co substitution. Hence, the positive impacts of melt spinning and Co substitution on the I_L value can be ascribed to the increased glass forming ability because an amorphous phase can markedly improves anti-corrosion and anti-oxidation abilities of the alloy electrode in a corrosive electrolyte [31], suggesting that the critical passivation current density of the alloy electrode is increased.

Based on above mentioned results, it can be concluded that both melt spinning treatment and the substitution of Co for Ni are beneficial for improving the hydrogen storage kinetics of the Mg_2Ni-type alloy.

5. Conclusions

The nanocrystalline and amorphous $Mg_2Ni_{1-x}Co_x$ ($x = 0, 0.1, 0.2, 0.3, 0.4$) alloy ribbons are successfully fabricated by melt spinning technology. The investigation of the structures of the alloys indicates that the substitution of Co for Ni facilitates the glass formation in the Mg_2Ni-type alloy. And the amorphization degree of the alloys visibly increases with increasing Co content. Both the melt spinning and Co substitution significantly improve the hydrogen storage kinetics of the alloys. The hydrogen absorption saturation ratio (R^a_t) and hydrogen desorption ratio (R^d_t) as well as the high rate discharge ability (HRD) increase with rising spinning rate and Co content. The hydrogen diffusion coefficient (D), the Tafel polarization curves and the electrochemical impedance spectra (EIS) measurements show that the electrochemical kinetics notably increases with rising spinning rate and Co content. Furthermore, all the as-spun alloys, when the spinning rate reaches to 30 m/s, have nearly same hydrogen absorption kinetics, indicating that the hydrogen absorption kinetics of the as-spun alloy is predominately controlled by diffusion ability of hydrogen atoms.

Acknowledgements

This work is supported by National Natural Science Foundations of China (50871050 and 50961009), Natural Science Foundation of Inner Mongolia, China (2010ZD05) and Higher Education Science Research Project of Inner Mongolia, China (NJzy08071).

References

[1] I.P. Jain, C. Lal, A. Jain, Int. J. Hydrogen Energy 35 (2010) 5133–5144.
[2] I.P. Jain, Int. J. Hydrogen Energy 34 (2009) 7368–7378.
[3] H. Simchi, A. Kaflou, Int. J. Hydrogen Energy 34 (2009) 7724–7730.
[4] L.J. Huang, G.Y. Liang, Z.B. Sun, Y.F. Zhou, J. Alloys Compd. 432 (2007) 172–176.
[5] P. Palade, S. Sartori, A. Maddalena, G. Principi, S. Lo Russo, M. Lazarescu, G. Schinteie, V. Kuncser, G. Filoti, J. Alloys Compd. 415 (2006) 170–176.
[6] R. Janot, X. Darok, A. Rougier, L. Aymard, G.A. Nazri, J.-M. Tarascon, J. Alloy Compd. 404–406 (2005) 293–296.
[7] N. Recham, V.V. Bhat, M. Kandavel, L. Aymard, J.-M. Tarascon, A. Rougier, J. Alloys Compd. 464 (2008) 377–382.
[8] H. Gu, Y.F. Zhu, L.Q. Li, Int. J. Hydrogen Energy 34 (2009) 7707–7713.
[9] H. Gu, Y.F. Zhu, L.Q. Li, Int. J. Hydrogen Energy 34 (2009) 2654–2660.
[10] M. Anik, J. Alloys Compd. 486 (2009) 109–114.
[11] D. Kyoi, T. Sakai, N. Kitamura, A. Ueda, S. Tanase, J. Alloy Compd. 463 (2008) 306–310.
[12] G. Liang, J. Alloys Compd. 370 (2004) 123–128.
[13] M.Y. Song, S.N. Kwon, J.S. Bae, S.H. Hong, Int. J. Hydrogen Energy 33 (2008) 1711–1718.
[14] M. Savyak, S. Hirnyj, H.-D. Bauer, M. Uhlemann, J. Eckert, L. Schultz, A. Gebert, J. Alloys Compd. 364 (2004) 229–237.
[15] K. Tanaka, T. Miwa, K. Sasaki, K. Kuroda, J. Alloys Compd. 478 (2009) 308–316.
[16] T. Spassov, U. Köster, J. Alloy Compd. 279 (1998) 279–286.
[17] G.K. Williamson, W.H. Hall, Acta Metall. 1 (1953) 22–31.
[18] G. Zhang, B.N. Popov, R.E. White, J. Electrochem. Soc. 142 (1995) 2695–2698.
[19] H. Niu, O. Derek, Northwood, Int. J. Hydrogen Energy 27 (2002) 69–77.
[20] N. Kuriyama, T. Sakai, H. Miyamura, I. Uehara, H. Ishikawa, T. Iwasaki, J. Alloys Compd. 202 (1993) 183–197.
[21] S.I. Yamaura, H.Y. Kim, H. Kimura, A. Inoue, Y. Arata, J. Alloys Compd. 339 (2002) 230–235.
[22] A. Inoue, T. Masumoto, Mater. Sci. Eng. A 173 (1993) 1–8.
[23] H.S. Chen, Acta Metall. 22 (1974) 1505–1511.
[24] Y.H. Zhang, B.W. Li, H.P. Ren, Z.H. Ma, S.H. Guo, X.L. Wang, Int. J. Hydrogen Energy 35 (2010) 2385–2392.
[25] Y. Wu, W. Hana, S.X. Zhou, M.V. Lototsky, J.K. Solberg, V.A. Yartys, J. Alloys Compd. 466 (2008) 176–181.
[26] Y. Takahashi, H. Yukawa, M. Morinaga, J. Alloys Compd. 242 (1996) 98–107.
[27] Y.H. Zhang, B.W. Li, H.P. Ren, S.H. Guo, Z.W. Wu, X.L. Wang, Int. J. Hydrogen Energy 34 (2009) 2684–2691.
[28] A. Gasiorowski, W. Iwasieczko, D. Skoryna, H. Drulis, M. Jurczyk, J. Alloys Compd. 364 (2004) 283–288.
[29] B.V. Ratnakumar, C. Witham, R.C. Bowman Jr., A. Hightower, B. Fultz, J. Electrochem. Soc. 143 (1996) 2578–2584.
[30] Y.F. Liu, H.G. Pan, M.X. Gao, Y.F. Zhu, Y.Q. Lei, Q.D. Wang, Int. J. Hydrogen Energy 29 (2004) 297–305.
[31] Y.H. Zhang, S.H. Guo, Y. Qi, X. Li, Z.H. Ma, Y. Zhang, J. Alloys Compd. 506 (2010) 749–756.